2013 IEEE/RSJ International Conference on
Intelligent Robots and Systems (IROS)
November 3-7, 2013. Tokyo, Japan

Personal Robot Assisting Transportation to Support Active Human Life

– Posture Stabilization based on Feedback Compensation of Lateral Acceleration –

Noriaki Hirose[1], Ryosuke Tajima[1] and Kazutoshi Sukigara[1]

Abstract— **Recently, a super-aging society has developed in many countries around the world. The research and development of PRs (personal robots) that improve the quality of human life is needed in order to accommodate the aging society. Elderly people will be able to spend their lives happily and effortlessly with the aid of useful and convenient PRs. However, excessive or premature use of PRs may cause health deterioration or contribute to the quick aging phenomenon. In this paper, a new prototype PR is proposed that can follow human beings with their baggage. Elderly people, therefore, will be able to go outside empty handed to shop, enjoy the fresh air, and visit friends. This PR will encourage people to walk outside and can eventually support an active lifestyle in its true sense. For actual use, PRs should have both a small footprint for coexistence in human society and high traveling performance for following the human wherever they go. Active posture control for the roll and pitch angles is applied to the PR to realize these requirements. The proposed structure and control approach using lateral acceleration as a control variable is verified by experiment using the new prototype robot.**

I. INTRODUCTION

Recently, a super-aging society has developed in many countries around the world. The research and development of PRs (personal robots) that improve the quality of human life is needed in order to accommodate the aging society [1]. Elderly people will be able to spend their lives happily and effortlessly with the aid of useful and convenient PRs. However, excessive or premature use of PRs may cause health deterioration or contribute to the quick aging phenomenon. Fig. 1[a] is an overview of a new prototype PR that can follow human beings and carry their baggage, as shown in Fig. 1[b]. Elderly people, therefore, will be able to go outside empty handed to shop, enjoy the fresh air, and visit friends. This PR will encourage people to walk outside and can eventually support an active lifestyle in its true sense.

In order to be able to follow human beings, there are two essential characteristics that PRs must have.

- a small footprint
- high traveling performance

A small footprint is needed for coexistence in human society. However, the small footprint results in a high center of gravity and deteriorates the traveling performance [2].

In this paper, a new prototype PR that can control the posture (the pitch and roll angles) is proposed to solve the above problem. Specifically, the control approach for the roll angle using lateral acceleration is described in detail.

[1]N. Hirose, R. Tajima, and K. Sukigara are with Intelligent Systems Lab., Information & Electronics Research Div., Toyota Central R & D Labs., Inc., 41-1 Yokomichi, Nagakute, Aichi, JAPAN hirose at mosk.tytlabs.co.jp

[a] front view [b] following human being

Fig. 1. Overview of Personal Robot.

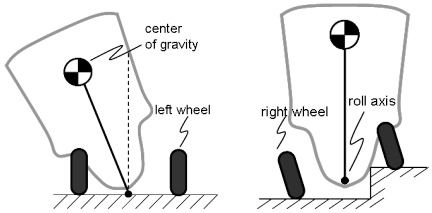

[a] turning [b] bumpy road

Fig. 2. Target behavior of PR for roll axis.

This control approach has a benefit over the conventional approach using the posture angle as the control variable [2][3][4][5][6][7][8] , in which the centripetal acceleration cannot be correctly measured. Moreover, the proposed approach can decrease the number of high-performance sensors needed to accurately estimate the roll angle. According to the proposed approach, the stable roll angle shown in Fig. 2[a] is automatically realized during a turning motion, and the vertical posture shown in Fig. 2[b] can also be realized, even on an uneven surface. The effectiveness of the proposed approach is verified by experiment using the new prototype PR.

II. MECHANICAL SYSTEM

A. Actuators

In Fig. 3, [a] shows a 3D drawing of the posture actuators used to control the roll and pitch angles of the PR, and [b] shows a lateral view. The right and left wheels are driven by motors with gears to stabilize the pitch angle using wheeled inverted pendulum control [9][10][11] . On the other hand, the roll angle of the PR can also be controlled around the roll axis using a motor with a gear (roll actuator) to realize quick turning and a vertical posture on an uneven surface. The roll actuator is designed with better backdrivability, less friction, and a smaller gear ratio to improve the posture

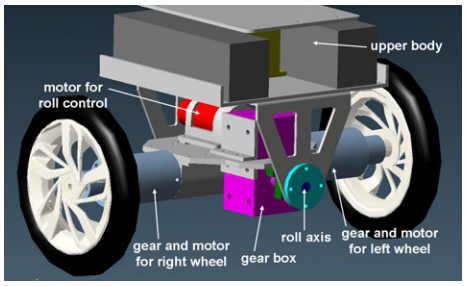

[a] 3D drawing sheet

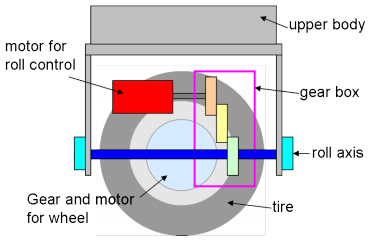

[b] lateral view

Fig. 3. Structure for posture actuator.

stabilization on an uneven surface. Because the disturbance force depends on the uneven surface, which deteriorates the posture stabilization, it is applied to the upper body of the PR through the roll actuator.

B. Sensors

In order to control the posture of the PR and evaluate the proposed control approach, an IMU (inertial measurement unit) is mounted on the upper body of the PR to detect the triaxial acceleration, angular velocity and posture angle (VG440 - Crossbow). In our experimental setup, the origin is defined on the ground at the center point between the wheels. In addition, the coordinate system is given as follows: the x axis is the traveling direction, the y axis is the direction to the left wheel from the origin, and the z axis is the vertical direction from the ground. The angular velocities of the right and left wheels are measured by encoders equipped on the right and left motors to realize wheeled inverted pendulum control.

Additionally, two laser range finders (UTM-30LX - HOKUYO) and two omnidirectional cameras (VS-C14 - Vstone) are equipped at the upper front and upper rear of the PR for tracking the human. However, the human tracking method is not discussed in this paper.

III. POSTURE CONTROL SYSTEM

A. Overview of Posture Control System

Fig. 4 shows a block diagram of the entire control system used by the PR to realize the desired traveling velocity v and turning velocity ω under posture stabilization. Here, v_{ref} and ω_{ref} indicate the references of v and ω, $\dot{\theta}_L$ and $\dot{\theta}_R$ indicate the angular velocities of the left and right wheels, $\dot{\theta}_x$ and $\dot{\theta}_y$ indicate the angular velocities of the upper body around the x and y axes, a_y indicates the described acceleration of

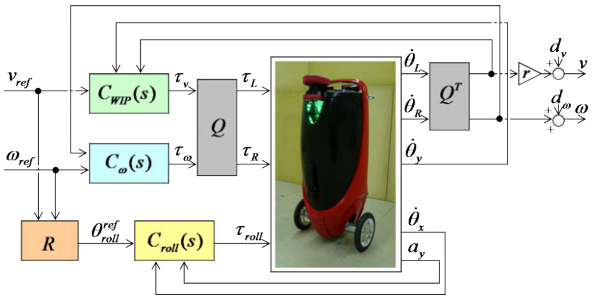

Fig. 4. Block diagram for posture control.

the upper body (lateral acceleration), $C_{WIP}(s)$ indicates the feedback controller for wheeled inverted pendulum control, $C_\omega(s)$ indicates the feedback controller for the turning velocity, $C_{roll}(s)$ indicates the proposed posture controller for the roll angle based on lateral acceleration, τ_v and τ_ω indicate the control inputs generated by $C_{WIP}(s)$ and $C_\omega(s)$, τ_L and τ_R indicate the torque inputs for the left and right wheels, and τ_{roll} indicates the torque input for the roll actuator. In addition, the constant matrix Q in Fig. 4 is defined as follows:

$$Q = \begin{bmatrix} \frac{1}{2} & -\frac{r}{d} \\ \frac{1}{2} & \frac{r}{d} \end{bmatrix}, \tag{1}$$

where $r(= 0.10)$ is the radius of the wheels, and $d(= 0.4)$ is the tread of the PR. Also, R generates the following roll angle reference θ^{ref}_{roll} in order to balance the centripetal acceleration $v \cdot \omega$ and acceleration due to gravity g during a steady turn:

$$\theta^{ref}_{roll}(t) = -\tan^{-1}\frac{v_{ref}(t) \cdot \omega_{ref}(t)}{g}. \tag{2}$$

At the above desired roll angle for $v_{ref} = v$ and $\omega_{ref} = \omega$, the ZMP (zero-moment point) is controlled at the origin to realize the most stable posture. However, the reference in (2) may not realize the desired roll angle when the fluctuation of the surface environment, the change in tire conditions, or individual mechanical differences happen the disturbance d_v and d_ω in Fig. 4 and cause $v_{ref} \neq v$ and $\omega_{ref} \neq \omega$. In order to solve the above problem, feedback compensation using the lateral acceleration $C_{roll}(s)$ is proposed in III-B.

On the other hand, $C_{WIP}(s)$ and $C_\omega(s)$ can be designed using the robust control theory based on a disturbance observer. However, the practical design method of $C_{WIP}(s)$ and $C_\omega(s)$ is not discussed in this paper.

B. Feedback Compensation of Lateral Acceleration

1) Purpose of Posture Control: Fig. 5 shows the front view of the PR model during a left turn. Here, $a(= v \cdot \omega)$ is the centripetal acceleration, O is the origin, z' and y' define the coordinate system for the upper body of the PR, and θ_{roll} is the roll angle. As shown in (2), the following desired roll angle θ_{roll} can be defined by substituting $v_{ref} = v$ and $\omega_{ref} = \omega$:

$$\theta_{roll}(t) = -\tan^{-1}\frac{a(t)}{g} = -\tan^{-1}\frac{v(t) \cdot \omega(t)}{g}. \tag{3}$$

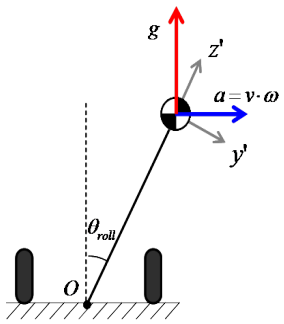

Fig. 5. Approximated model for roll axis.

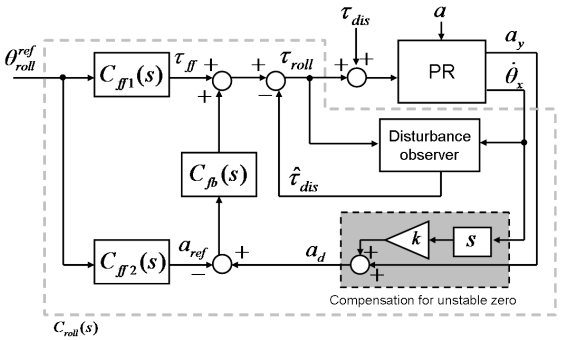

Fig. 6. Block diagram for feedback control system $C_{roll}(s)$.

Here, the centripetal acceleration $a(= v \cdot \omega)$ is not known. Therefore, the roll angle reference θ_{roll}^{ref} in (2) is given using v_{ref} and ω_{ref} instead of v and ω. In the conventional control approach, which controls the roll angle as a control variable [4][5], the reference in (2) is given to the control system to realize the above roll angle. However, the desired roll angle cannot be realized because $v \neq v_{ref}$ and $\omega \neq \omega_{ref}$ when the surface condition fluctuates, the tire pressure is decreased, or individual mechanical difference occurs. In addition, the roll angle θ_{roll} should be estimated using a high-performance gyro sensor and an acceleration sensor in the conventional approach. High-cost sensors are not required for actual use. In this paper, feedback compensation for the acceleration in the y' axis direction (lateral acceleration a_y) is proposed to realize the desired roll angle in (3). Now, a_y can be expressed as follows:

$$a_y(t) = g\sin\theta_{roll}(t) + a(t)\cos\theta_{roll}(t) - h\ddot{\theta}_{roll}(t), \quad (4)$$

where $h(= 0.4)$ is the distance between the origin O and the center of gravity. By substituting (3) and $\ddot{\theta}_{roll} = 0$ into (4), (4) can be modified as follows:

$$a_y(t) = g\sin\theta_{roll}(t) + a(t)\cos\theta_{roll}(t) = 0. \quad (5)$$

Equation (5) means that zeroing the lateral acceleration a_y can produce the desired roll angle in (3).

2) Subject for Lateral Acceleration Feedback: The transfer function of the plant system from τ_{roll} to the lateral acceleration a_y is given to design the feedback controller

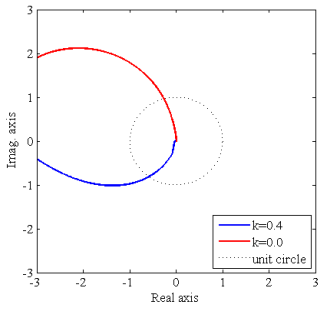

Fig. 7. Nyquist diagram.

$C_{roll}(s)$. At first, the equation of motion around the x axis is expressed as follows:

$$\begin{aligned} J\ddot{\theta}_{roll}(t) &= \tau_{roll}(t) + Mgh\sin\theta_{roll}(t) \\ &\quad -Mha(t)\cos\theta_{roll}(t), \end{aligned} \quad (6)$$

where $J(= 2.85)$ is the inertia around the x axis, and $M(= 18.0)$ is the weight of the upper body. (6) can be linearized for $\theta_{roll} \ll 1$.

$$J\ddot{\theta}_{roll}(t) = \tau_{roll}(t) + Mgh\theta_{roll}(t) - Mha(t) \quad (7)$$

Equation (7) can be modified by Laplace transformation as follows:

$$\theta_{roll}(s) = \frac{1}{Js^2 - Mgh}\tau_{roll}(s) - \frac{Mh}{Js^2 - Mgh}a(s). \quad (8)$$

The transfer function from the control input τ_{roll} to θ_{roll} (the plant system for the conventional control approach) can be expressed as follows:

$$\frac{\theta_{roll}(s)}{\tau_{roll}(s)} = \frac{1}{Js^2 - Mgh}. \quad (9)$$

On the other hand, the linearized (4) for $\theta_{roll} \ll 1$ can be modified by Laplace transformation.

$$a_y(s) = -h(s^2 - \frac{g}{h})\theta_{roll}(s) + a(s) \quad (10)$$

By substituting (10) into (9), the following transfer function (the plant system for the proposed approach) can be generated:

$$\frac{a_y(s)}{\tau_{roll}(s)} = -h\frac{s^2 - \frac{g}{h}}{Js^2 - Mgh} \quad (11)$$

From (11), the transfer function includes zeros for $\pm\sqrt{\frac{g}{h}}$. Specifically, $+\sqrt{\frac{g}{h}}$ is an unstable zero that limits the control bandwidth [12]. The value of $+\sqrt{\frac{g}{h}}$ is +4.95 [rad/s] in the PR. Therefore, it is difficult for the PR to realize the control bandwidth target because the unstable zero of +4.95 [rad/s] is too close to the control bandwidth target of 6.28 [rad/s] (= 1.0 [Hz]). The unstable zero deteriorates the stability margin and destabilizes the feedback control system.

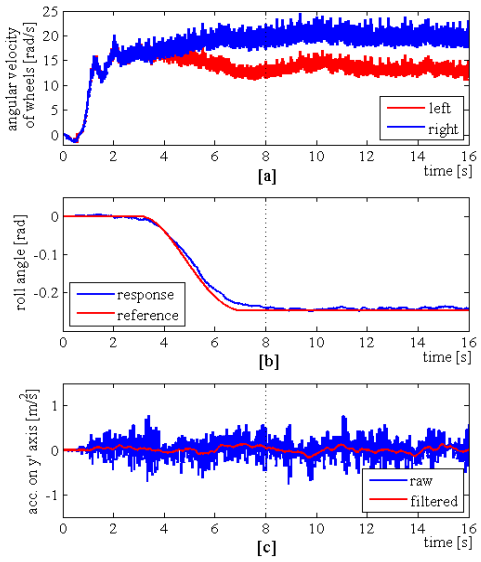

Fig. 8. Experimental results (1.67 [m/s], 1.6 [rad/s]).

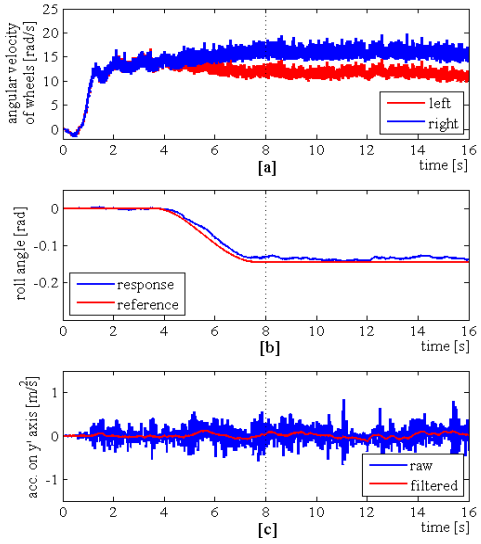

Fig. 9. Experimental results (1.39 [m/s], 1.06 [rad/s]).

3) Compensation for Unstable Zero: In order to realize the control bandwidth target, the unstable zero has to be reassigned at the higher frequency range. Now, the value a_d is defined as the control variable (instead of a_y) as follows:

$$a_d(t) = a_y(t) + k\ddot{\theta}_{roll}(t). \tag{12}$$

Here, $k > 0$ is a free parameter. As shown in (5), the sum of the first and second terms on the right-hand side of (4) should be zero at the desired roll angle (3). In addition, the third term on the right-hand side of (4) causes a lower unstable zero in (11). The transfer function from τ_{roll} to a_d can be

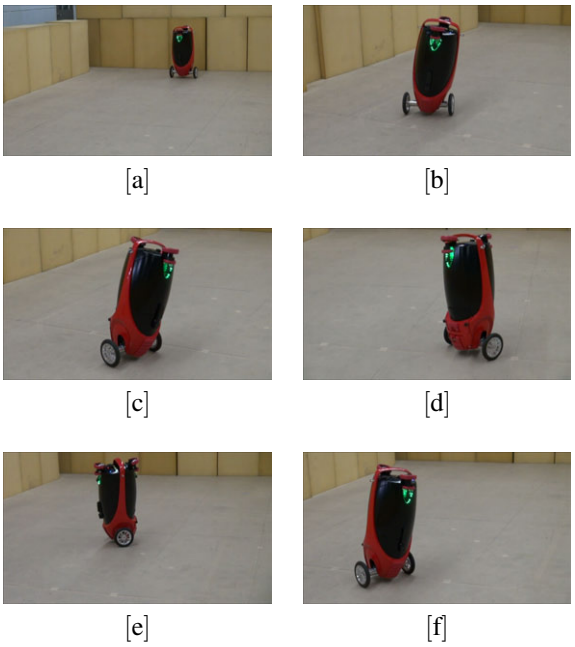

Fig. 10. Snapshot of turning experiment.

expressed as follows by substituting (12) into (11),

$$\frac{a_d(s)}{\tau(s)} = -(h-k)\frac{s^2 - \frac{g}{h-k}}{Js^2 - Mgh}, \tag{13}$$

where the zeros $\pm\sqrt{\frac{g}{h-k}}$ in (13) are definitely larger than $\pm\sqrt{\frac{g}{h}}$. The control bandwidth target can be realized if k is determined to be $\pm\sqrt{\frac{g}{h-k}}$ and is much larger than 6.28 [rad/s]. For $|h-k| \ll 1$, (13) can be redefined as follows:

$$\frac{a_d(s)}{\tau(s)} = \frac{g}{Js^2 - Mgh}. \tag{14}$$

There are no unstable or stable zeros in (14) under the ideal condition of $|h-k| \ll 1$. In addition, the difference between (9) and (14) is only the steady gain g.

To compensate for the unstable zero in (12), $\ddot{\theta}_{roll}$ can be obtained from the derivation of $\dot{\theta}_x$, which is measured using the gyro sensor. The control variable a_d in (12), therefore, can easily be generated by one acceleration sensor for a_y and one gyro sensor for $\dot{\theta}_x$.

4) Design of Feedback Controller $C_{roll}(s)$: Fig. 6 shows a block diagram of the feedback control system $C_{roll}(s)$. The "disturbance observer," $C_{fb}(s)$, $C_{ff1}(s)$, and $C_{ff2}(s)$ are designed as follows:

- "Disturbance observer"
  The roll actuator includes coulomb and viscous friction. Additionally, the PR has perturbations in J, h, and M when loading the baggage. These disturbances, described as τ_{dis} in Fig. 6, deteriorate the positioning performance and control stability. The "disturbance observer" is applied to compensate for τ_{dis} in order to improve the robust control performance. The following

approximated model is designed for the "disturbance observer" and the to-be-described feedforward compensations $C_{ff1}(s)$ and $C_{ff2}(s)$:

$$J\ddot{\theta}_{roll}(t) = \tau_{roll}(t). \tag{15}$$

In this approximated model, the second term on the right-hand side of (6) equals the third term. The estimated disturbance $\hat{\tau}_{dis}$ can be given as follows:

$$\begin{aligned} \hat{\tau}_{dis}(s) &= Q(s) \cdot (Js\dot{\theta}_x(s) - \tau(s)), \\ Q(s) &= \frac{{\omega_{ob}}^2}{s^2 + 2\zeta_{ob}\omega_{ob}s + {\omega_{ob}}^2}, \end{aligned} \tag{16}$$

where $\omega_{ob} = 2 \cdot \pi \cdot 2.0$, and $\zeta_{ob} = 0.95$. This observer can accurately estimate values below 2.0 [Hz].

- $C_{fb}(s)$
  $C_{fb}(s)$ is the feedback controller for the control variable a_d. The following PD controller and low-pass filter are applied:

$$\begin{aligned} C_{fb}(s) &= (K_p + K_d \cdot s) \cdot C_a(s), \\ C_a(s) &= \frac{\omega_a}{s + \omega_a}, \end{aligned} \tag{17}$$

  where K_p and K_d are the feedback gains, and ω_a is designed to be $2 \cdot \pi \cdot 10$ to reduce the sensor noise. K_p and K_d are selected to stabilize the feedback control system.
- $C_{ff1}(s)$, $C_{ff2}(s)$
  In order to improve the following performance at the transient response, a two-degree-of-freedom control system is one efficient technique[13]. The feedforward compensations $C_{ff1}(s)$ and $C_{ff2}(s)$ are designed as follows using the approximated model in (15):

$$\frac{\tau_{ff}(s)}{\theta^{ref}_{roll}(s)} = C_{ff1}(s) = J \cdot s^2 \cdot C_b(s), \tag{18}$$

$$\frac{a_{ref}(s)}{\theta^{ref}_{roll}(s)} = C_{ff2}(s) = g \cdot C_b(s) - g, \tag{19}$$

  where τ_{ff} indicates the feedforward torque input, a_{ref} indicates the reference of the lateral acceleration, and $C_b(s)$ is designed as follows to be the proper transfer function for $C_{ff1}(s)$ and $C_{ff2}(s)$:

$$C_b(s) = \left(\frac{\omega_b^2}{s^2 + 2\zeta_b\omega_b s + \omega_b^2} \right)^2, \tag{20}$$

  where $\omega_b = 2 \cdot \pi \cdot 2.0$, and $\zeta_b = 0.95$. According to the above design, θ_{roll} can be expressed as follows when the approximated model in (15) coincides with the actual plant system:

$$\theta_{roll}(s) = C_b(s)\theta^{ref}_{roll}(s). \tag{21}$$

  As a result, the feedback compensation $C_{fb}(s)$ can be activated when a perturbation occurs.

Each compensation that is designed as a continuous system is discretized by the bilinear Z-transform and is implemented into MicroAutoBox - dSPACE.

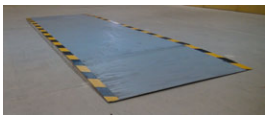

[a] overview

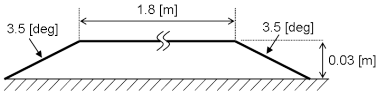

[b] side view

Fig. 11. Configuration of uneven surface in experiment.

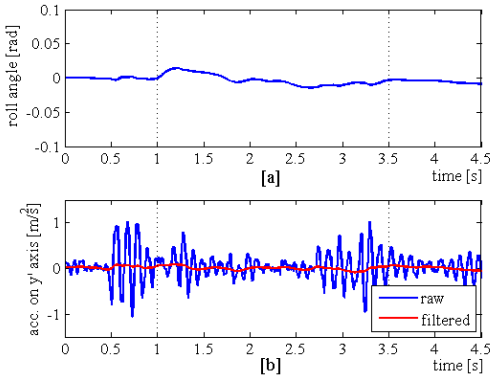

Fig. 12. Experimental results on 0.03 mm bump.

5) Evaluation of Stability Margin: Fig. 7 shows the Nyquist diagram for the proposed control system in Fig. 6. The blue line is the Nyquist locus of $k = 0.4$, the red line is the Nyquist locus of $k = 0.0$ without compensation for the unstable zero, and the dotted black line is a unit circle. The blue line with the compensation for the unstable zero ensures the stability margin and realizes a robust control system. On the other hand, it is confirmed that the red line without the compensation of the unstable zero has a large amount of phase delay from the unstable zero, and the control system is unstable.

IV. Experimental Results

The effectiveness of the proposed posture control approach is verified using two kinds of experiments. The first experiment is for quick turning on a flat surface. The roll angle reference θ^{ref}_{roll} is given by (2) in this experiment.

The second experiment is for traveling on an uneven surface. Only the left-side tire travels on the uneven surface constructed with a slope and a 0.03 [m] bump for $\theta^{ref}_{roll} = 0$ and $\omega_{ref} = 0$.

A. Quick Turning on Flat Surface

Fig. 8 show the experimental results for turning left at $v_{ref} = 1.67$ [m/s] and $\omega_{ref} = 1.6$ [rad/s]. In Fig. 8, [a] indicates the angular velocities of the wheels, [b] indicates the roll angle, and [c] indicates the lateral acceleration. In

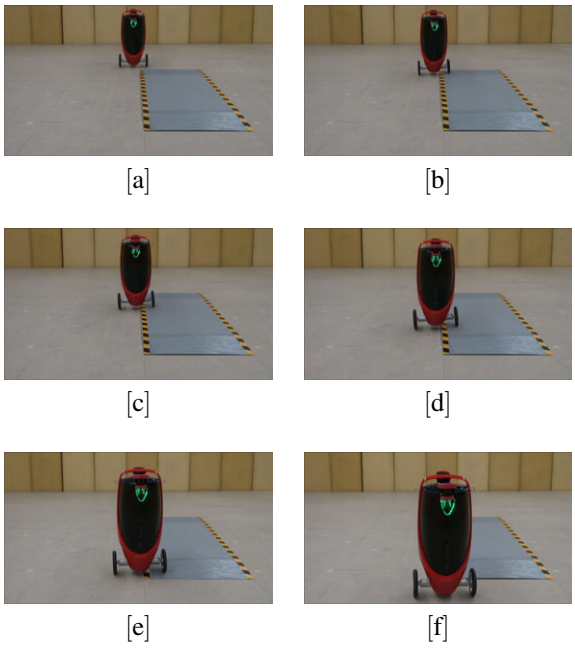

Fig. 13. Snapshot of experiment on slopes

each figure, the vertical dotted line indicates 8.0 [s]. From Fig. 8[a], ω_{ref} makes a difference between the angular velocity of the left wheel (shown as a red line) and the angular velocity of the right wheel (shown as a blue line) from 4.0 [s] on. Also, the PR is turning at a steady rate after 8.0 [s]. In Fig. 8[b], the blue line for the roll angle θ_{roll} settles at a steady value after 8.0 [s]. Also, the lateral acceleration a_y can be controlled to zero to realize an appropriate roll angle, although the centripetal acceleration a is $0.3\times g(= 1.67 \times 1.6)$. Moreover, in Fig. 8[b], there is a small steady error during steady turning between the blue line and the red line of the reference. This error indicates the benefit of the proposed feedback compensation using lateral acceleration. The proposed control approach can automatically compensate for the error in the centripetal acceleration between $v \cdot \omega$ and $v_{ref} \cdot \omega_{ref}$.

On the other hand, Fig. 9 show the experimental results for turning left at $v_{ref} = 1.39$ [m/s] and $\omega_{ref} = 1.06$ [rad/s]. The centripetal acceleration during the steady turn is $0.15\times g$ in this experiment. In the same way as in Fig. 8, the desired roll angle for the centripetal acceleration $0.15\times g$ is achieved by zeroing the lateral acceleration. Fig. 10 shows snapshots of the experiment in Fig. 8. The behavior of the PR, which is controlled around the roll axis, is confirmed.

B. Traveling on Uneven Surface

In Fig. 11, [a] shows an overview of the uneven surface used in the experiment, and [b] shows a side view. In the experiment, only the left-side tire goes over this surface, and it does so at $v = 1.11$ [m/s]. The conventional robot without posture actuator makes a fluctuation of roll angle, which is assumed 0.075 [rad] $(= \sin^{-1}\frac{0.03}{d})$, on this environment. In Fig. 12, [a] shows the experimental data for the roll angle θ_{roll}, and [b] shows the experimental data for the lateral acceleration a_y. In each figure, the vertical dotted lines indicate 1.0 [s] and 3.5 [s]. From 1.0 [s] to 3.5 [s], the left-side tire of the PR is on the uneven surface.

Although only the left tire is on the 0.03 [m] bump, the roll angle can be settled at about 0.0 [rad] by zeroing the lateral acceleration a_y. And, the maximum value of roll angle at transient state can be also suppressed at 0.014 [rad]. It is much smaller than 0.075 [rad] without posture actuator. Fig. 13 shows snapshots of the experiment in Fig. 12. Even on the uneven surface, the PR can maintain a vertical posture.

V. CONCLUSION

In this paper, the mechanical system of our new prototype robot was presented, and a posture stabilization approach based on feedback compensation of lateral acceleration was proposed. The proposed control approach can realize the desired roll angle, even when the surface condition and tire pressure fluctuate. The effectiveness of the proposed approach was verified using two kinds of basic experiments: quick turning on a flat surface and traveling on an uneven surface. Two important future works are remained: (1) applying the preview control approach of the ZMP for the improvement of the transient traveling performance, and (2) dealing with the fluctuation of the inertia and the center of gravity when loading and unloading the baggage.

REFERENCES

[1] M. Yamaoka, Personal Mobility Robot, Journal of the Robotics Society of Japan, Vol.26, No.8, pp.27–28, 2008.
[2] Y. Hosoda, S. Egawa, J. Tamamoto, K. Yamamoto, R. Nakamura, and M. Togami, Basic Design of Human-Symbiotic Robot EMIEW, Proc. of the 2006 IEEE/RSJ International Conference on Intelligent Robots and Systems, pp. 5079–5084, 2006.
[3] M. Morita, and A. Yanaka, "Personal Mobility i-REAL", Journal of Society of Automotive Engineers of Japan, Vol.66, No.12, pp.36–41, 2012.
[4] R. Rajamani, J. Gohl, L. Alexander, and P. Starr, Dynamics of Narrow Tilting Vehicle, Mathematical and Computer Modeling of Dynamical Systems, Vol.9, No.2, pp. 209–231, 2003.
[5] D. Piyabongkarn, T. Keviczky, and R. Rajamani, "Active Tilt Control for Stability Enhancement of a Narrow Commuter Vehicle", International Journal of Automotive Technology, Vol.5, No.2, pp. 77–88, 2004.
[6] M. Krid, and F. Benamar, Design and control of an active anti-roll system for a fast rover, Proc. of the 2011 IEEE/RSJ International Conference on Intelligent Robots and Systems, pp. 274–279, 2011.
[7] http://www.lumeneo.fr/
[8] http://www.icona-stc.com/
[9] T. Takei, R. Imamura, and S. Yuta, Baggage Transportation and Navigation by a Wheeled Inverted Pendulum Mobile Robot, IEEE Trans. on Industrial Electronics, Vol. 56, No. 10, pp. 3985–3994, 2009.
[10] A. Shimada, and N. Hatakeyama, High-Speed Motion Control of Wheeled Inverted Pendulum Robots, Proc. of 4th IEEE International Conference on Mechatronics, pp. 1–6, 2007.
[11] N. Hirose, K. Sukigara, H. Kajima, and M. Yamaoka, Mode Switching Control for a Personal Mobility Robot based on Initial Value Compensation, Proc. of the 36th Annual Conference of the IEEE Industrial Electronics Society, pp.1908–1913, 2010.
[12] J.S. Freudenberg, and D.P. Looze, Right Half Plane Poles and Zeros and Design Tradeoffs in Feedback Systems, IEEE Trans. on Automatics Control, Vol.AC-30, No.6, pp.555–565, 1985.
[13] N. Hirose, M. Iwasaki, M. Kawafuku, and H. Hirai, Deadbeat Feedforward Compensation with Frequency Shaping in Fast and Precise Positioning, IEEE Trans. on Industrial Electronics, Vol. 56, No.10, pp. 3790 – 3797, 2009.